Effect of mixing the low-valence transition metal atoms Y = Co, Fe, Mn, Cr, V, Ti, or Sc on the properties of quaternary Heusler compounds $Co_{2-x}Y_xFeSi$ ($0 \leqslant x \leqslant 1$)

R. Mahat,[1,*] U. Karki,[1] Shambhu KC,[1] J. Y. Law,[2] V. Franco,[2] I. Galanakis,[3,†] A. Gupta,[4] and P. LeClair[1,‡]

[1]*Department of Physics and Astronomy, The University of Alabama, Tuscaloosa, Alabama 35487, USA*

[2]*Departamento de Física de la Materia Condensada ICMSE-CSIC, Universidad de Sevilla, Sevilla 41080, Spain*

[3]*Department of Materials Science, School of Natural Sciences, University of Patras, GR-26504 Patras, Greece*

[4]*Department of Chemistry and Biochemistry, The University of Alabama, Tuscaloosa, Alabama 35487, USA*

(Received 4 April 2022; accepted 9 June 2022; published 29 June 2022)

In this paper we report an experimental study of structural, magnetic, and mechanical properties of quaternary Heusler alloys $Co_{2-x}Y_xFeSi$ (Y = Co, Fe, Mn, Cr, V, Ti, or Sc, $0 \leqslant x \leqslant 1$) and the experimental findings are supported by *ab initio* electronic structure calculations. The alloys were synthesized using an arc-melting technique. Single phase microstructures are observed for all alloys substituted with low-valence transition metals Y except Sc. X-ray powder diffraction patterns at room temperature show the presence of Heusler-like face-centered cubic crystal structure in all single phase specimens. The low-temperature saturation magnetic moments, as determined from magnetization measurements, agree fairly well with our theoretical results and also follow the Slater-Pauling rule of thumb for half-metals, a prerequisite for half-metallicity. The alloys are predicted to exhibit half-metallic ferromagnetism by *ab initio* electronic structure calculations using the GGA+U approach. All stable compounds are observed to have high Curie temperatures with linear dependence with the valence electrons concentration in the alloys. Relatively high hardness values are also measured, approaching 15.7 GPa for Ti-substituted material, highest among the values reported for Heuslers so far. All these properties strongly suggest the alloys are promising for the spintronic applications at room temperature and above.

DOI: 10.1103/PhysRevMaterials.6.064413

I. INTRODUCTION

Co_2-based full Heusler compounds belong to a promising class of materials for magnetoelectronics applications because of their potential for half-metallic ferromagnetism (and resulting 100% spin polarization), high Curie temperatures, lattice matching with conventional semiconductors, and properties easily tuned through substitution. With stoichiometric composition Co_2YZ, Y is usually another transition metal and Z is a main group element, and compounds typically crystallize in the cubic $L2_1$ structure (space group $Fm\bar{3}m$ [1,2]). The main features of interest here—the potential for half-metallicity—is an exceptional electronic structure, one with an energy band gap at the Fermi level (E_F) only for minority spin electrons [3–7], which would yield 100% spin polarization at the Fermi level. However, the experimentally observed spin polarization is always much smaller than 100%. The discrepancy between theory and experiment is expected to be due to structural and chemical disorder [8,9]. Improvements in various properties such as structure, magnetization, transport, critical temperature T_c, magnetoresistance, as well as high spin polarization can be realized in somewhat disordered Heusler alloys by the substitution of a fourth element, with the quaternary analogs observed to have reduced structural disorder. The elemental substitution also alters the degree of hybridization between the $3d$ orbitals of different elements, with consequent changes in the position of the Fermi level with respect to the spin subbands [10–15]. That is, adding a fourth element may serve to not only further stabilize the structure and reduce disorder, it may also help tune the properties of interest to more desirable values.

In previous studies, the doping of low-valent transition metal atoms in ternary Heusler alloys has been reported to open the minority spin energy gap around Fermi level, giving 100% spin polarization and stabilizing a half-metallic state [16,17]. Our earlier work included a number of series based on Co_2FeGe [18–20], substituting for both Co and Fe, and clearly demonstrating both the ability to stabilize single phase material and tune electronic and magnetic properties. The Co_2FeSi (CFS) parent is even more attractive as a starting point for applications due to its larger magnetic moment of 6 μ_B/f.u. and high Curie temperature of 1100 K [5]. However, the half-metallicity in the parent compound is perhaps still an open question, as both half-metallic [21] and non-half-metallic [4] properties have been reported theoretically. Kandpal *et al.* [21] reported half-metallic band structure calculations using local spin density approximation and generalized gradient approximation, including optimum effective Coulomb exchange interaction (U_{eff}). On the other hand, Galanakis *et al.* [4] reported a non-half-metallic state using the full-potential screened Korringa-Kohn-Rostoker Green's function approach. In that case, the Fermi level fell on the edge of the minority conduction band, leading to unstable

*rmahat@crimson.ua.edu
†galanakis@upatras.gr
‡pleclair@ua.edu

half-metallicity. Naturally, half-metallic ferromagnets with a stable energy gap in minority spin channel are desired for technical applications, particularly when one considers finite temperature effects [22,23]. If the Fermi energy is near one of the band edges, the energy gap may easily be smeared out at finite temperatures or destroyed by quasiparticle excitations [22,23]. To achieve robustness, compounds with Fermi level located at the middle of the minority energy gap are highly preferred [22,23]. As such, there is great utility in being able to slightly shift the position of the Fermi level in a system that is nearly half-metallic to stabilize a robust half-metallic state, or to improve the robustness of a marginal half-metal. This is where quaternary substitution can play a decisive role: if Co_2FeSi is not *quite* a stable half-metal, can the gentle substitution of a fourth element push it toward a stable half-metallic state? And, at the same time, can this also improve other useful properties that have led people to this system, such as magnetic or thermoelectric characteristics?

This is the basic starting point for the present work: if one of the Co atom in Co_2FeSi is substituted by another lower valence transition metal atom Y = Fe, Mn, Cr, V, Ti, or Sc, a spectrum of alloys with rich and useful properties can be generated. In fact this idea is already well understood in the Heusler alloys in general. The inverse Heusler alloy Fe_2CoSi (which one could view as $Co_{2-x}Fe_{1+x}Si$ with $x = 1$) has been reported to be zero-gap half-metal with very low Gilbert damping [24,25]. The quaternary Heusler CoFeMnSi has been observed theoretically and experimentally to be a spin-gapless semiconductor [26–28], CoFeCrSi has been reported to be half-metallic with some structural disorder [29], while CoFeVSi and CoFeTiSi are reported theoretically to be nearly half-metallic and half-metallic respectively, but both have been observed experimentally to show multiphase behavior in bulk form [30,31]. In all these quaternary Heusler alloys, the Fermi level lies on the edge of the minority valence band. As we go from Co_2FeSi to CoFeYSi, for a lower valence substituent Y, the Fermi level is shifted from the lower edge of the conduction band to the upper edge of the valence band in the minority spin channel, in accordance with the calculations by Galanakis *et al.* [32]. They suggested that an expansion of the lattice should shift the Fermi level lower in energy, while a contraction of the lattice should shift it higher. Since one can expect robust half-metallicity with Fermi level exactly in the middle of the minority spin band gap, this gives us a prescription for a potentially marginal half-metal Co_2FeSi. Since according to Galanakis *et al.* the Fermi level fell on the edge of the minority conduction band, we would like to move the Fermi level lower in energy, and this means a lattice expansion. This in turn means that if we substitute a lower valence Y element with larger atomic radius than Co [33] in $Co_{2-x}Y_xFeSi$, we should be able to move the Fermi level toward midgap. The substitution of a Y atom for Co in Co_2FeSi may then be also seen as d-electron deficiency.

There have already been several detailed studies on Co_2FeSi showing that substitution plays an important role in realizing useful electronic and magnetic properties and tuning the Fermi level towards the center of the minority band gap [10,22,34–36]. The band gap at the Fermi level can be varied by substituting a fourth element at any of the three $X/Y/Z$ sites, i.e., $Co_{2-x}Y^*_xYZ$, $Co_2Y_{1-x}Y^*_xZ$, or $Co_2YZ_{1-x}Z^*_x$ where Y, Y^* are low-valence transition elements and Z, Z^* are main group elements [9,37–42]. Substitution at X/Y site is perhaps more convincing as the X/Y site elements play the main role in tailoring the half-metallicity and magnetic properties compared to the Z site element [32]. For example: Cr substitution for Fe in Co_2FeSi has been observed to increase the spin polarization [10]; low Gilbert damping has been observed in a half-metallic $Co_2Fe_xMn_{1-x}Si$ substitutional series [35]; and the tuning of Fermi level for half-metallicity has been demonstrated in Heusler alloy $Co_2FeAl_{0.5}Si_{0.5}$ [34,36]. It is the aim of this work to synthesize Co_2FeSi and investigate the effect of low-valence transition metal (Y = Fe, Mn, Cr, V, Ti, or Sc) substitution for Co on structural, electronic, magnetic, and mechanical properties.

II. METHODS

A. Experimental methods

Polycrystalline $Co_{2-x}Y_xFeSi$ (Y = Co, Fe, Mn, Cr, V, Ti, or Sc, $0 \leqslant x \leqslant 1$) off-stoichiometric Heusler alloys were prepared by conventional arc melting of constituents of 99.99% purity on a water-cooled Cu hearth under argon flow, with a base pressure of 10^{-4} mbar. The mixture was flipped and melted at least 6 times to ensure chemical homogeneity. Ti was melted inside the vacuum chamber separately as an oxygen getter before melting the compound to avoid oxygen contamination. The weight loss during the process was less than 1%. The resulting ingots were cut into pieces and examined using an energy dispersive x-ray spectroscopy (EDS) detector equipped in a JEOL 7000 field emission scanning electron microscope (FESEM) to ensure the target composition after the arc melting. These pieces were annealed in evacuated quartz tubes for different heat treatments, and cooled slowly in the furnace to get optimum crystallization to promote the formation of $L2_1$ structure. To make the comparison uniform across all compositions, only the samples annealed under similar heat treatments (i.e., 900 °C for 7 days) are reported. The heat treatments were followed by metallography (see details in the Supplemental Material of our previous publications [43,44]) to produce a metallic shiny surface for microstructure analysis by optical and electron microscopes. After heat treatment and metallography, the composition and homogeneity of the samples were again confirmed by EDS.

The crystal structure was investigated by means of x-ray diffraction (XRD) using a Bruker D8 Discover x-ray diffractometer equipped with monochromatic Co-$K\alpha$ (λ = 0.179 nm) radiation at room temperature. The specimens were crushed by hand using a mortar and pestle, and the XRD measurements were carried out on the crushed powder samples by rotating around the ϕ axis to minimize surface effects. It should be noted that ball milling can result in a distortion of the crystalline structure due to mechanical robustness of our alloys (discussed in a subsequent section). CaRIne crystallography 4.0 software [45] as well as in-house PYTHON code [46] including the dispersive corrections to the atomic scattering factors were used to simulate the XRD patterns to compare with the experimental XRD patterns. Rietveld refinements of the XRD data were performed using MATCH! software based

on the FullProf algorithm [47]. Magnetization isotherms at 5 and 300 K were studied by means of Quantum Design Physical Properties Measurement System (PPMS) using small spherical sample pieces of ∼20–30 mg, while the high temperature magnetization was measured using LakeShore VSM 7407. The mechanical properties in terms of Vickers hardness were measured by using Buehler model 1600–6100 microhardness tester.

B. Computational methods

Ab initio calculations are performed using density-functional theory (DFT) employing the projector augmented wave (PAW) pseudopotentials by Blöchl [48], implemented by Kresse and Furthmüller in the Vienna *ab initio* simulation package (VASP) [49]. We have adopted the generalized-gradient approximation (GGA) as formulated by Perdew, Bueke, and Ernzerhof (PBE) for the electronic exchange-correlation potential [50]. A 16-atom supercell, i.e., 4 formula units of the underlying $L2_1$ structure adopted by the perfect full-Heusler compounds like Co_2MnGe is used in all of our calculations. The integrals in the reciprocal space of cubic systems was done considering a $20 \times 20 \times 20$ Γ-centered Monkhorst-Pack grid [51] using the linear tetrahedron method with Blöchl corrections. Total energies were converged up to 10^{-7} eV/cell with a cutoff for the kinetic energy of the plane waves of 520 eV. Full relaxation of cell (initially cubic) volume, shape, and atomic positions were performed until the forces on each atom become less than 10^{-2} meV/cell using the conjugate-gradient method. Spin-orbit interaction is ignored in our calculations as it is not crucial for the half-metallic properties of Heusler compounds [52].

Ab initio electronic structure calculations using GGA approach in the case of parent compound CFS with 30 valence electrons per formula unit has been reported to predict a significantly reduced magnetic moment with respect to experiment and the Slater-Pauling value, due to the well-known on-site electronic correlations of the *d* electrons and related fractional state occupation [21]. The observed half-metallic properties of CFS is reported to be recovered by introducing an appropriate Hubbard U term into the electronic Hamiltonian [21]. In our study we have also presented GGA+U calculations on $Co_{2-x}Y_xFeSi$ system and explore how the CFS electronic properties are affected by low-valence atomic substitutions.

The Hubbard U parameter cannot be calculated simultaneously with the minimization of the total energy because total energy remains constant with respect to the U term. Both experimental and computational determination of the U values are very difficult and tedious tasks. In 2013 Sasioglu and collaborators employed the constrained random-phase approximation (CRPA) scheme to calculate the U values for several half-metals [53]. For the calculations presented in the rest of this work, we have used the semiempirical values mentioned in Ref. [54], where Kandpal *et al.* have employed the LDA+U scheme to study the electronic structure of several half-metallic Heusler compounds. The U values used for the *d* orbitals of Co, Fe, Mn, Cr, V, Ti, and Sc are 1.92, 1.80, 1.69, 1.59, 1.34, 1.36, and 1.30 eV, respectively. Finally, it should be noted that the inclusion of U artificially opens a band gap in the minority spin channel and only comparison to experimental data guarantees that the U parameters used in the calculations are adequate for a particular material.

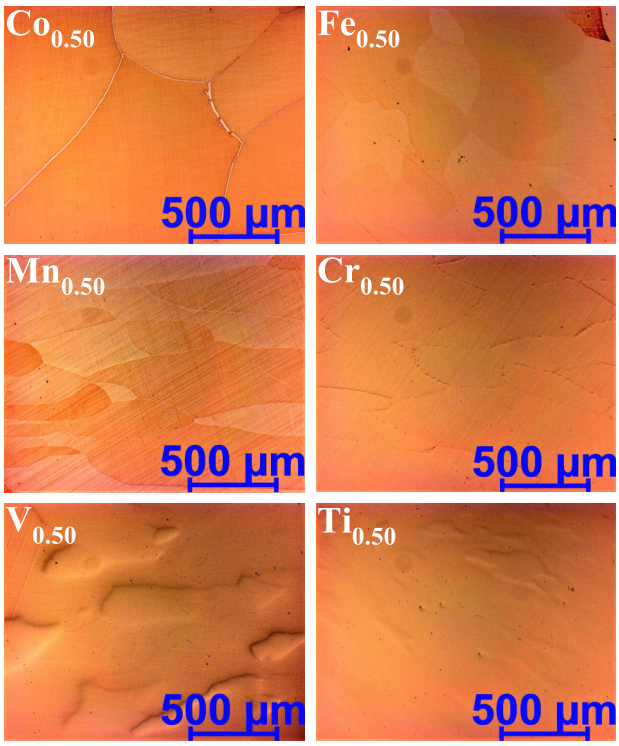

FIG. 1. Optical micrograph of $Co_{2-x}Y_xFeSi$ (Y = Co, Fe, Mn, Cr, V, or Ti, $x = 0.50$) annealed at 900 °C for 7 days followed by slow cooling showing the granular microstructure. The samples were etched for 60 s using the Adler etchant.

III. RESULTS AND DISCUSSIONS

A. Experimental results and discussions

1. Microstructural and compositional analysis

Optical microscopy and SEM of polished and etched samples are very helpful to characterize the microstructure specially when the impurity phase contents are either below the detection limit of XRD (less than roughly 5% of the overall volume) or amorphous in nature [18,19,55,56]. These methods provide a morphological image which can clearly expose secondary phases and grain boundary segregation even for minor constituents. We can first speculate the presence of impurity phases by observing areas of different contrast in optical microscopy, and subsequently SEM with EDS can be utilized to quantify whether regions of different contrasts truly have different compositions or are, for instance, just different crystallite orientations.

Figure 1 shows the microstructures of all single phase specimens $Co_{2-x}Y_xFeSi$ (Y = Co, Fe, Mn, Cr, V, or Ti, $x = 0.50$) annealed at 900 °C for 7 days, observed using an optical microscope. With the substitution of 50% Y content (Co, Fe, Mn, Cr, V, Ti, or Sc) for Co in Co_2FeSi, we observed single phase microstructures except for 50% Sc. Our results are in accordance with previous reports for 50% Co and Fe for Co in Co_2FeSi. It is found that the grain size of the alloys decreased

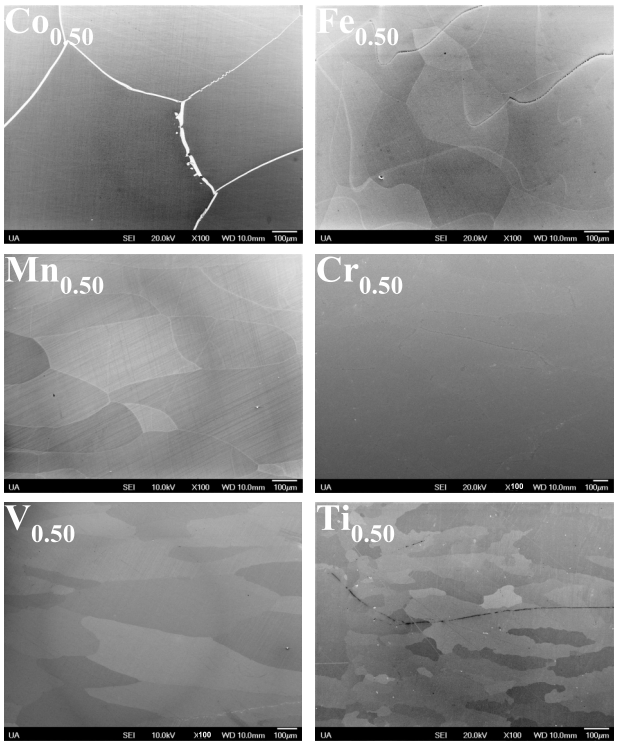

FIG. 2. SEM micrograph of $Co_{2-x}Y_xFeSi$ (Y = Co, Fe, Mn, Cr, V, or Ti, $x = 0.50$) alloys annealed at 900 °C for 7 days followed by slow cooling, showing the granular microstructure.

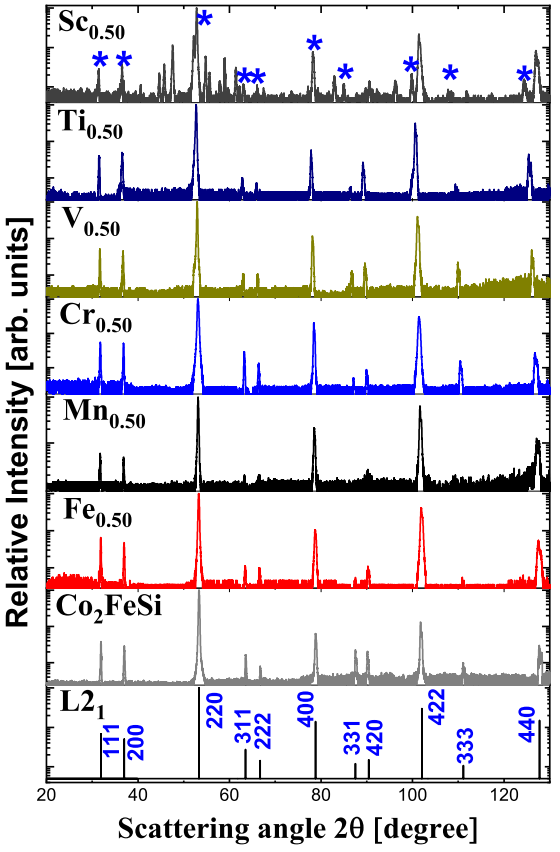

FIG. 3. Experimental XRD patterns of $Co_{2-x}Y_xFeSi$ (Y = Co, Fe, Mn, Cr, V, Ti or Sc, $x = 0.50$) alloy series annealed at 900 °C for 7 days investigated at room temperature, here $*$ corresponds to Heusler cubic peaks in Sc-based alloy while others are from secondary phase/unknown impurity phase. The first from the bottom is the simulated XRD pattern for ordered $L2_1$ structure of Co_2FeSi. The relative intensity (y axis) is plotted in log scale so that all the peaks can be seen clearly.

greatly with the substitution of less valence Y content. The contrast developed in micrograph (see Figs. 1–5 in the Supplemental Material [57]) suggests significant compositional differences between phases in the case of 50% Sc for Co. The composition was measured to differ from the target composition by more than 5% with the secondary phase mainly located in grain boundaries. The stoichiometry within the grains of all the single-phase specimens was confirmed as the target composition within an instrumental uncertainty of ∼5% using EDS (see Table I in the Supplemental Material [57]).

Figure 2 shows the typical electron images displaying the microstructure of single phase alloys. The optical and electron micrographs of all the remaining alloys in the series are presented in the Supplemental Material [57].

2. *Crystal structure and atomic order analysis*

The structural and chemical order of the alloys is important for their potential use in any kind of spintronics applications, and to this end structural analysis has been performed with XRD. Figure 3 shows the powder XRD spectra of the studied alloys with $x = 0.50$, measured at room temperature, using a Co-K_α radiation source (see Fig. 6 in the Supplemental Material [57]). All the alloys showed single phase behavior except for Sc, consistent with microstructures observed in previous section. For the Sc sample, asterisks denote possible Heusler cubic peaks while other peaks are from secondary phases/unknown impurity phases. All the XRD peaks in single-phase alloys can be indexed to a face-centered cubic (fcc) structure, with h, k, l all odd or even. As expected only three distinct types of peaks are observed: fundamental peaks with $h + k + l = 4n$, even superlattice peaks with $h + k + l = 4n + 2$, and odd superlattice peaks with $h + k + l = 2n + 1$. Heusler alloys in the ordered $L2_1$ structure are characterized by the presence of superlattice reflection (SR) peaks; the presence of (111) peak indicates the chemical ordering of atoms in octahedral positions, and (200) peak indicates the order for atoms in tetrahedral positions, while the (220) peak is a principal reflection which is independent of the state of the order [58].

In full Heusler alloys (FHA) of the type X_2YZ in the $L2_1$ structure, Z is the main group element with highest electronegativity which occupies 4a (0,0,0) Wyckoff sites in the $Fm\bar{3}m$ space group, Y is the lower valence transition metal atom with smallest electronegativity and occupies the 4b($\frac{1}{2}$, $\frac{1}{2}$, $\frac{1}{2}$) Wyckoff sites, and the transition metal X atoms are of intermediate electronegativity and occupy the 8c($\frac{1}{4}$, $\frac{1}{4}$, $\frac{1}{4}$) Wyckoff sites [corresponding to the 4c($\frac{1}{4}$, $\frac{1}{4}$, $\frac{1}{4}$), and 4d($\frac{3}{4}$, $\frac{3}{4}$, $\frac{3}{4}$) Wyckoff positions in the "half Heusler" $C1_b$ structure of space group $F\bar{4}3m$] [8,59]. Hereafter, we refer to the 4a and 4b sites as the A sublattice and 4c and 4d together as the B sublattice, as shown in Fig. 4. The intensities of superstructure peaks are affected by various types of

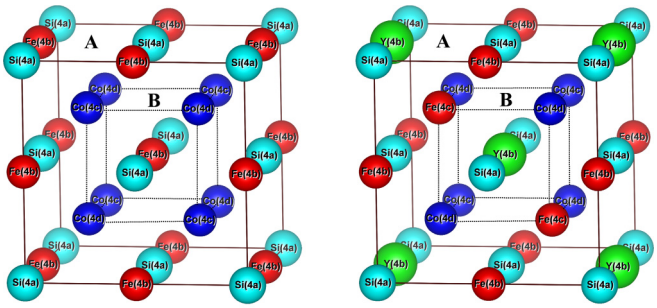

(a) (b)

FIG. 4. Crystal structure in a unit cell of (a) CFS and (b) $Co_{1.50}Y_{0.50}FeSi$ (Y = Fe, Mn, Cr, V, Ti, or Sc) (I) configuration mentioned in Table I assuming $L2_1$ structure. The structures are shown in their ideal, unrelaxed forms.

atomic disorders, e.g., (i) A2 (bcc) disorder due to random distribution of atoms over lattice sites 4a, 4b, 4c, and 4d which results in vanishing superstructure peaks, (ii) B2 (CsCl) disorder due to random distribution between atoms in 4a and 4b sites which results only the (200) superstructure peak and vanishing (111) peak, and (iii) DO_3 (BiF_3) disorder when disorder is between atoms in 4b, 4c, and 4d sites only [60]. This disordered structure DO_3 results in a (111) peak with much higher intensity than the (200) peak. All these types of disorder would destroy the half-metallic property of the material by introducing density of states (DOS) at Fermi level in the minority spin channel [41], even though the magnetic moment of the materials may still follow a Slater-Pauling rule.

As shown in Fig. 3 (see also Fig. 8 in the Supplemental Material [57]), the superlattice reflection peaks (111) and (200) are clearly visible as expected for the defect-free ordered Heusler structure (the degree of chemical ordering has been obtained using the Webster's model [61] as discussed in Sec. I B of the Supplemental Materials [57]), indicating the presence of a long range ordering in all single phase specimens. The measured and expected values for I_{111}/I_{220} and I_{200}/I_{220} are observed to agree with each other qualitatively (see Fig. 8 in the Supplemental Material [57]).

In order to gain more insight on chemical ordering, we performed Rietveld refinement of experimental XRD pattern for $Co_{2-x}Y_xFeSi$ (Y = Co, Fe, Mn, Cr, V, or Ti, x = 0.50) considering three nondegenerate configurations as presented in Table I. Details of the refinements for the best fit configuration (I) are provided in Table II. The observed, calculated and difference profiles for the best fit configuration (I) after performing the Rietveld refinement are provided in the Supplemental Material [57]. The crystal structure for

TABLE I. Possible site assignments for cubic $Co_{2-x}Y_xFeSi$ (Y = Co, Fe, Mn, Cr, V, Ti, or Sc, x = 0.50) Heusler system.

Type	4a (0,0,0)	4b $(\frac{1}{2},\frac{1}{2},\frac{1}{2})$	4c $(\frac{1}{4},\frac{1}{4},\frac{1}{4})$	4d $(\frac{3}{4},\frac{3}{4},\frac{3}{4})$
I	Si	$Fe_{0.50}Y_{0.50}$	$Co_{0.50}Fe_{0.50}$	Co
II	Si	$Co_{0.50}Y_{0.50}$	Fe	Co
III	Si	Fe	$Co_{0.50}Y_{0.50}$	Co

TABLE II. Goodness of fit parameters (χ^2 and R_{Bragg} factor) obtained from Rietveld refinement for $Co_{2-x}Y_xFeSi$ (Y = Co, Fe, Mn, Cr, V, or Ti, x = 0.50) alloys.

Y element	χ^2	R_{Bragg}
Co	1.1	5.3
Fe	1.3	6.9
Mn	1.5	11.2
Cr	1.9	9.1
V	1.6	8.3
Ti	1.5	7.7

this configuration is shown in Fig. 4(b) (see Fig. 9 in the Supplemental Material [57] for other possible configurations). In this configuration, we presumed that low-valence Y substituent atoms will displace Fe atoms from 4b sites towards vacated Co sites, and Y atoms will subsequently fill the sites previously occupied by Fe. This results in Y atoms forming an ionic-type sublattice with Si, which has a larger electronegativity, rather than with Co and Fe and the system becomes stable by Y donating its electrons to other elements in the alloy. The Co and displaced Fe atoms have intermediate electronegativities and occupy tetrahedral sites [8,59]. In other words, Co and Fe atoms are assumed to be on the tetrahedral sublattice B (4c and 4d) and Fe, Y, and Si on the octahedral sublattice A (4a and 4b). This Hume-Rothery condition of phase stability of substitutional solid solution also supports this atomic configuration. According to this rule, the atomic size difference between two elements should be no larger than 15% and electron negativity difference no higher than 0.4 in order to form the stable solid solution [62–64]. However, complementary measurements like neutron diffraction, synchrotron x-ray diffraction techniques which are capable of differentiating elements that are close to Fe/Co are required to better understand the chemical ordering in the crystal lattice. We used Cohen's method with a Nelson-Riley extrapolation to accurately determine the lattice parameters from XRD data [66]. The dependence of the lattice parameter a on the Y content for $Co_{2-x}Y_xFeSi$ (Y = Co, Fe, Mn, Cr, V, or Ti, $0 \leqslant x \leqslant 1$) is shown in Fig. 5(a) while Fig. 5(b) shows the variation of lattice parameter with atomic number of Y ele-

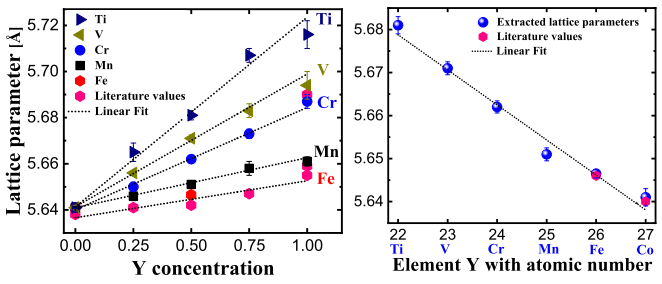

(a) (b)

FIG. 5. Variation of lattice parameter with (a) Y content in $Co_{2-x}Y_xFeSi$ (Y = Co, Fe, Mn, Cr, V, or Ti, $0 \leqslant x \leqslant 1$), and (b) atomic number of low-valence transition metal element Y in $Co_{2-x}Y_xFeSi$ (Y = Co, Fe, Mn, Cr, V, or Ti, x = 0.50) showing linear behavior. The pink data points represent literature values [5,65].

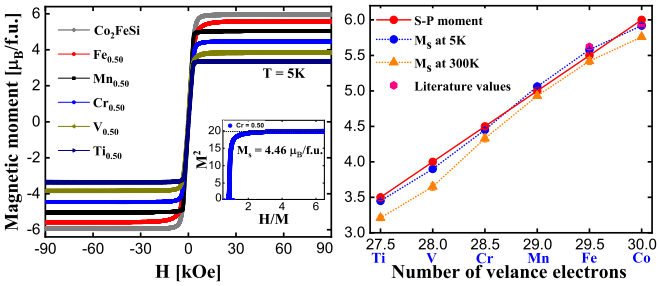

FIG. 6. (a) Isothermal magnetization curves of $Co_{2-x}Y_xFeSi$ (Y = Co, Fe, Mn, Cr, V, or Ti, $x = 0.50$) at 5 K. (b) The saturation magnetic moment versus valence electron counts per formula units with element Y, both experimental (at 5 and 300 K) and expected from the Slater-Pauling rule for half-metals. The pink data points represent reported literature values [5,65].

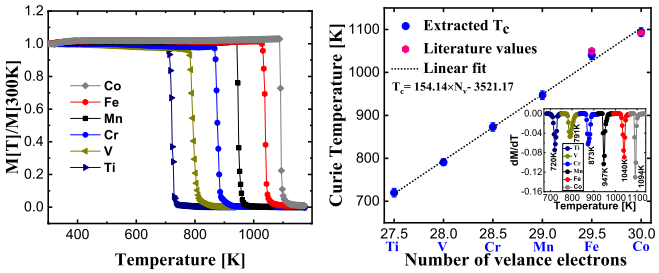

FIG. 7. (a) Temperature dependence of magnetization at 100 Oe, and (b) variation of Curie temperature as a function of valence electron counts per formula units with element Y ($x = 0.50$). The inset shows the first-order derivative of magnetization as a function of temperature, the minima of which is used to extract T_c. The pink data points represents reported literature values [5,65].

ment in $Co_{1.50}Y_{0.50}FeSi$ (Y = Co, Fe, Mn, Cr, V, or Ti). It is noticed that the lattice parameter increases linearly with the substitution of less valence Y content, consistent with Vegard's law [67] as atomic radii decrease in the order Ti > V > Cr > Mn > Fe > Co [33].

3. Magnetic characterization

Most of the Co-based half-metallic Heusler alloys show a Slater-Pauling-like behavior for the magnetization when crystallized in a fully ordered state [68]. The Slater-Pauling (SP) rule relates the dependence of the magnetic moment with the valence electron concentration (Z_t) following a simple electron counting scheme for ordered, half-metallic ferromagnetic Heusler compounds. If the value of the saturation magnetization changes with Y element according to the Slater-Pauling rule of thumb for half-metals, then we expect the total magnetization to be [4,8]

$$M_t = [(2 - x)Z_{Co} + xZ_Y + Z_{Fe} + Z_{Si}] - 24, \qquad (1)$$

where M_t is the total spin magnetic moment per f.u. in μ_B and Z_i is the number of valence electrons of each individual atom. In $Co_{2-x}Y_xFeSi$ (Y = Co, Fe, Mn, Cr, V, or Ti, $0 \leqslant x \leqslant 1$) system, the total number of valence electrons change from 30 in CFS to 25 in CoFeTiSi. Therefore, the SP behavior predicts that the saturation magnetic moment should decrease with the substitution of Y element for Co. Specifically, a saturation magnetic moment of

$$M(Y) = 6 - x(Z_{Co} - Z_Y) \qquad (2)$$

is thus expected for $Co_{2-x}Y_xFeSi$.

For magnetic properties, we primarily used the VSM option of a Quantum Design PPMS Dynacool working in the temperature range of $T = 5$ to 400 K and with maximum magnetic field of 9 T to observe low temperature magnetizations for all single-phase alloys. Figure 6(a) shows the isothermal magnetization curves measured at 5 K for $x = 0.50$ (see Figs. 11–13 in the Supplemental Material [57] for magnetization curves of all other alloys in the series), as expected for ferromagnets. All the alloys are saturated in a magnetic field of about 4 kOe which indicates small magnetocrystalline anisotropy in the specimens. The Arrot plot method [69] (i.e., by linear extrapolation to $H/M = 0$ of M^2 versus H/M curves) was utilized to determine the spontaneous magnetizations [see inset to Fig. 6(a)]. Total saturation magnetic moments (M_s) obtained from the spontaneous magnetization at 5 K are observed to follow the Slater-Pauling rule of thumb for half-metals (see red data points) and decrease with the decrease of valence electrons in Y atoms [see Fig. 6(b)]. The decrease of M_s is expected due to the decrease in the number of Co atoms. The magnetic moment per formula unit for $x = 0$, i.e., CFS, is measured to be 5.92 μ_B, which is also in good agreement with reported results [5,65]. The systematic variation of saturation magnetic moments with Y atom concentration ($0 \leqslant x \leqslant 1$) in the series is provided in Fig. 14 in the Supplemental Material [57]. The slight deviation of magnetic moments from expected Slater-Pauling values could be due to the slight variation in the stoichiometry of the alloys, weighing and measurement errors, partial surface oxidation, and the measurement temperature of 5 K. The experimentally determined magnetic moments are also in good agreement with those obtained from first-principle calculations (see Table IV), as discussed in a forthcoming section.

Figure 7(a) shows the temperature dependent specific magnetization of the alloys for $x = 0.50$ (see Fig. 14 in the Supplemental Material [57] for all other alloys in the series), measured by means of a vibrating sample magnetometer (LakeShore VSM 7407) equipped with a high temperature stage. We present the results above 300 K so that the behavior close to the Curie temperature T_c is not masked by the rapid decrease of the magnetization at lower temperatures. Moreover, the measurements were not performed at saturation but in a constant magnetic field of 100 Oe. This leads to a more drastic drop of the magnetization at the T_c but it allows the more precise determination of T_c which is our goal.

The Curie temperatures T_c were extracted from the inflection point, i.e., by taking the minima of the first-order derivative of $M(T)$ curves [see inset in Fig. 7(b)]. The Curie temperature is observed to decrease with the substitution of low-valence transition metal element Y due to the weakening of the exchange interaction caused by a small magnetic moment of substituted element Y compared to Co. The decrease in T_c can also be attributed to the increase in lattice parameter

TABLE III. Experimental lattice parameters and saturation magnetic moments at $T = 5$ K along with the Slater-Pauling (SP) values, and the measured Curie temperature (T_c) of $Co_{2-x}Y_xFeSi$ (Y = Co, Fe, Mn, Cr, V, or Ti, $0 \leqslant x \leqslant 1$) alloy series. The numbers in parentheses are the uncertainty in the last digit, e.g., 5.92(3) = 5.92 ± 0.03. Values in square brackets are taken from the literature.

Series	Concentration	Expt. lattice parameter (Å)	Expt. M_s (μ_B/f.u.)	SP (μ_B/f.u.)	T_c (K)	Vickers hardness (GPa)
Co_2FeSi	$x = 0$	$a = 5.641(2)$[5.636]	5.92(3)[6.00]	6.00	1094(10)[1100][5,70]	7.33(4)
$Co_{2-x}Fe_xFeSi$	$x = 0.25$	$a =$ [5.641]	[5.75]	5.60	[1058][65,70]	–
	$x = 0.50$	$a = 5.646(2)$[5.642]	5.58(2)[5.62]	5.50	1040(10)[1069][65,70]	7.55(6)
	$x = 0.75$	$a =$ [5.647]	[5.60]	5.20	[1052][65,70]	–
	$x = 1$	$a =$ [5.655]	[5.20]	5.00	[1036][65,70]	–
$Co_{2-x}Mn_xFeSi$	$x = 0.25$	$a = 5.646(2)$	5.57(4)	5.50	–	7.51(4)
	$x = 0.50$	$a = 5.651(2)$	5.06(3)	5.00	947(10)	7.94(3)
	$x = 0.75$	$a = 5.658(3)$	4.49(2)	4.50	869(10)	8.51(5)
	$x = 1$	$a = 5.661(2)$	4.03(3) [3.99]	4.00	761(10)[763]	9.69(7)
$Co_{2-x}Cr_xFeSi$	$x = 0.25$	$a = 5.650(2)$	5.20(4)	5.25	969(10)	7.82(6)
	$x = 0.50$	$a = 5.662(1)$	4.46(3)	4.50	873(10)	8.61(8)
	$x = 0.75$	$a = 5.673(2)$	3.72(2)	3.75	790(10)	9.78(9)
	$x = 1$	$a = 5.687(3)$	2.91(2)[2.82]	3.00	710(10)	11.33(9)
$Co_{2-x}V_xFeSi$	$x = 0.25$	$a = 5.656(1)$	4.89(4)	5.00	924(10)	8.52(5)
	$x = 0.50$	$a = 5.671(1)$	3.90(3)	4.00	791(10)	9.85(7)
	$x = 0.75$	$a = 5.683(3)$	2.89(4)	3.00	553(10)	11.37(8)
	$x = 1^{\dagger}$	$a = 5.694(6)$	1.45(5)	2.00	345(10)	11.79(10)
$Co_{2-x}Ti_xFeSi$	$x = 0.25$	$a = 5.665(4)$	4.75(5)	4.75	902(10)	10.75(7)
	$x = 0.50$	$a = 5.681(2)$	3.45(2)	3.50	720(10)	12.58(3)
	$x = 0.75$	$a = 5.707(3)$	2.23(5)	2.25	487(10)	13.81(9)
	$x = 1$[a]	$a = 5.716(6)$	0.88(9)	1.00	331(10)	15.72(14)

[a]Multiphase specimen.

with the substitution of Y changing the distance between magnetic ions leading to a weak exchange interaction. A linear dependence is obtained when plotting T_c as a function of number of valence electron concentration, and hence M_s [see Fig. 7(b)], which is expected in half-metallic Co-based Heusler alloys [38]. According to this plot, T_c is the highest for those that exhibit a large magnetic moment, or equivalently for those with a high valence electron concentration as derived from the Slater-Pauling rule. The high values of T_c usually imply stable magnetism and half-metallicity over wide temperature range, necessary in practical applications. The systematic variation of Curie temperatures with Y atom concentration ($0 \leqslant x \leqslant 1$) in the series is provided in Fig. 14 in the Supplemental Material [57].

The experimental values of lattice parameters, saturation magnetic moments at 5 K, Curie temperatures, and corresponding mechanical hardness values of all single phase specimens in $Co_{2-x}Y_xFeSi$ (Y = Co, Fe, Mn, Cr, V, or Ti, $0 \leqslant x \leqslant 1$) alloy series are summarized in Table III.

4. Vickers microhardness

For industrial applications, materials require mechanical robustness to undergo repetitive thermal cycling and resist cracking from vibrations. Here we have measured the mechanical properties in terms of Vickers hardness. Figure 8(a) displays the variation of Vickers microhardness with transition metals of increasing atomic number in $Co_{2-x}Y_xFeSi$ (Y = Co, Fe, Mn, Cr, V, or Ti) series with $0 \leqslant x \leqslant 1$ and Fig. 8(b) shows the variation for allows with $x = 0.50$, all measured at room temperature. The corresponding harness values are given in Table III. The data were taken from at least 12 different regions of each sample with 0.2 kg load and 10 s loading time and average values are reported here. The Vickers hardness is calculated from

$$HV = 1.8544F/D^2 \text{ [kg/mm}^2\text{]}, \quad (3)$$

where D is the diagonal length of the impression of the diamond probe. Relatively high hardness values are measured, approaching 15.72 GPa for CoFeTiSi, highest among the values reported for Heuslers so far [18–20,43,44,71–73]. The hardness is observed to increase with the substitution of Y

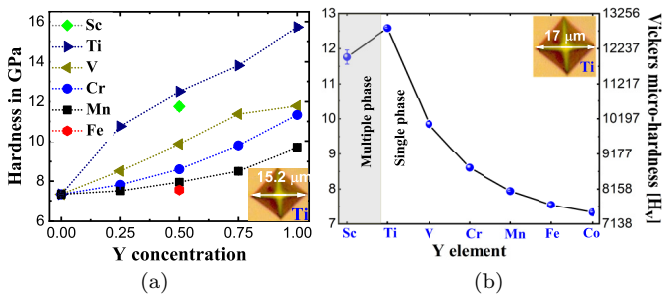

FIG. 8. Vickers hardness versus Y content in $Co_{2-x}Y_xFeSi$ (Y = Co, Fe, Mn, Cr, V, Ti, or Sc), all annealed at 900 °C for 7 days (a) for all the alloys $0 \leqslant x \leqslant 1$, and (b) for alloys with $x = 0.50$. The imprints of the indenter with radial cracks for Ti = 1 [bottom right of (a)] and Ti = 0.50 [top right of (b)] are shown.

TABLE IV. Parameters extracted from DFT calculations (both GGA and GGA+U approach) for type I configuration. In the table M, M_{SP}, $\langle a \rangle$, and Δ represent calculated magnetic moment, Slater-Pauling moment, optimized lattice parameter, and energy gap at Fermi level. The last column shows the tetragonality in the structure $a/c - 1$. The values in the parentheses represent the calculated values using GGA approach.

Y element	Configurations	4d	4c	4b	4a	M (μ_B/f.u.)	M_{SP} (μ_B/f.u.)	$\langle a \rangle$ (Å)	Tet. ($a/c - 1$)	Δ (eV)
Co	Co_8-Fe_4Si_4	4Co	4Co	4Fe	4Si	6.000(5.484)	6.000	5.636	0.012	0.791
Fe	Co_6Fe_2-Fe_4Si_4	4Co	2Fe,2Co	4Fe	4Si	5.502(5.369)	5.500	5.640	0.012	0.387
Mn	Co_6Fe_2-$Fe_2Mn_2Si_4$	4Co	2Fe,2Co	2Mn,2Fe	4Si	5.000(4.999)	5.000	5.645	0.012	0.575(0.138)
Cr	Co_6Fe_2-$Fe_2Cr_2Si_4$	4Co	2Fe,2Co	2Cr,2Fe	4Si	4.500(4.480)	4.500	5.657	0.012	0.626
V	Co_6Fe_2-$Fe_2V_2Si_4$	4Co	2Fe,2Co	2V,2Fe	4Si	3.999(3.856)	4.000	5.678	0.012	0.176
Ti	Co_6Fe_2-$Fe_2Ti_2Si_4$	4Co	2Fe,2Co	2Ti,2Fe	4Si	3.500(3.463)	3.500	5.690	0.012	0.597
Sc	Co_6Fe_2-$Fe_2Sc_2Si_4$	4Co	2Fe,2Co	2Sc,2Fe	4Si	3.000(2.994)	3.000	5.717	0.012	0.719

element of increasing atomic radius and depends on phases present as reported in the literature [74].

B. Theoretical results and discussions

The parent compound Co_2FeSi of the series $Co_{2-x}Y_xFeSi$ (Y = Co, Fe, Mn, Cr, V, Ti, or Sc, $x = 0.50$) has already been reported in the literature to form the $L2_1$ structure with a low degree of chemical disorder [22] and our experimental investigations confirmed the low-valence transition metals Y substitution for Co in Co_2FeSi also give stable single phases with XRD patterns consistent with the ordered $L2_1$ structure (except for scandium substituted alloy). These experimental facts allow us accurate comparison between experiment and theory. We note that DFT using the GGA approach predicts a significantly reduced magnetic moment with respect to experiment and Slater-Pauling values, but that the introduction of Hubbard U terms in the GGA approach, i.e., GGA+U, resolves the discrepancy in Co_2FeSi [21,22]. In order to predict the size and nature of band gaps and magnetic moments, we have therefore performed the electronic-structure calculations using both GGA and GGA+U approaches.

For theoretical calculations, bulk $Co_{1.50}Y_{0.50}FeSi$ (Y = Co, Fe, Mn, Cr, V, Ti, or Sc) cubic supercell structures consisting of 16 atoms were constructed using the Monte Carlo special quasirandom structure (MCSQS) method [75] which is a part of the open source ATAT toolkit [76] accessible from [77]. The MCSQS method can handle double-site substitutions as described in the experimental section above taking care of nearest neighbor interaction and predicts a special quasirandom structure by generating a set of clusters with specific correlations relative to a target random structure. The best MCSQS structures were confirmed after waiting for a long enough time until a correlation difference relative to the target random structure approaches zero. The predicted MCSQS structures are in good agreement with configuration I predicted in Table I [see also Fig. 4(b)]. The predicted MCSQS structures were then optimized using GGA method. The experimental lattice constants extracted in our experimental work were employed as starting values for the calculations. The optimized lattice parameters are in good agreement with experimental values, increasing with the substitution of atoms with low valency. All the calculated parameters are presented in Table IV.

Figure 9 shows the calculated spin polarized density of states (DOS) plots for majority and minority spin channels using both GGA (blue) and GGA+U (red) where the Fermi level is represented by the zero energy. Our calculations show the systematic shifting of Fermi level from conduction band edge in the parent compound Co_2FeSi towards the energy gap in minority spin channel after substituting low-valence transition metals (see Fig. 15 in the Supplemental Material [57]

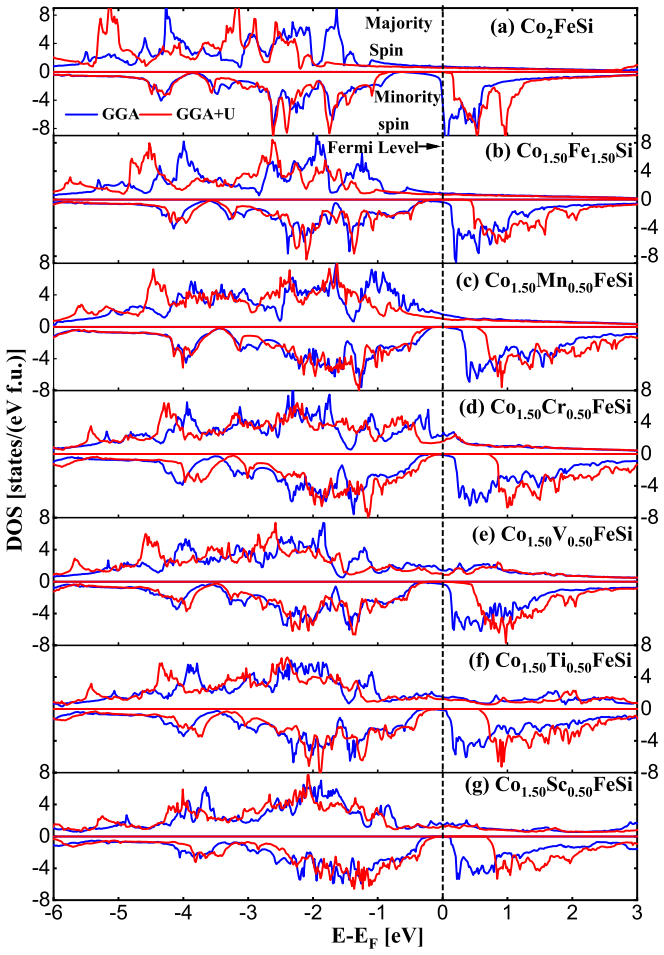

FIG. 9. Spin polarized total density of states (TDOS) of $Co_{1.50}Y_{0.50}FeSi$ (Y = Co, Fe, Mn, Cr, V, Ti, or Sc) alloys using both GGA (blue) and GGA+U (red) methods. Number of states in each plot is scaled with respect to 1 f.u.

for the atom-resolved DOS). In the GGA approach, only the $Co_{1.50}Mn_{0.50}FeSi$ alloy is observed to be a perfect half-metal with the Fermi level within the energy gap in the minority spin channel. Moreover, in the case of the $Co_{1.50}Cr_{0.50}FeSi$ alloy, the presence of the Cr atom leads to a peak in the majority spin d states in the vicinity of Fermi level consistent with previous observations [18,78,79]. The nonzero contribution to DOS from Fe(I) (which shares the same sublattice A with Y atoms) at Fermi level in the minority spin channel is observed to play a major role in destroying the half-metallicity in all other alloys. The inclusion of electron-electron correlation in GGA+U approach shifts the Fermi level within the gap for all compounds resulting in a half-metallic behavior. We should note that the minority spin energy band gap decreases as we substitute lower-valence transition metal atoms for Co in Co_2FeSi. The *ab initio* calculated energy gaps are provided in Table IV.

In Table III we provide the experimentally determined total spin magnetic moments in μ_B for all the samples which we have grown, and in Table IV we summarize the total spin magnetic moments calculated using both the GGA functional and the GGA+U approach for the $x = 0.5$ case. The inclusion of electron-electron correlation in the GGA+U approach opens the gap, as expected, in the minority spin channel, the Fermi level shifts within the gap for all compounds resulting in calculated total spin magnetic moments slightly larger than GGA ones and in almost perfect agreement with the ones predicted by the Slater-Pauling rule. Although differences between both GGA and GGA+U calculated values and the experimental ones are quite small, we expect that GGA+U performs slightly better than GGA since (a) calculations are done at 0 K and experimental magnetic moments were measured at 5 K and (b) samples have an intrinsic degree of disorder despite their very high crystallinity. Thus calculations should slightly overestimate the spin magnetic moments with respect to the experimentally measured ones.

IV. CONCLUSION

In summary, quaternary Heusler alloys $Co_{2-x}Y_xFeSi$ (Y = Co, Fe, Mn, Cr, V, Ti, or Sc, $0 \leqslant x \leqslant 1$) were synthesized and a combined experimental and theoretical study of structural, electronic, magnetic, and mechanical properties of quaternary Heusler alloys $Co_{2-x}Y_xFeSi$ (Y = Co, Fe, Mn, Cr, V, Ti, or Sc, $x = 0.50$) were carried out. The alloys were identified as potential half-metallic ferromagnets by *ab initio* electronic structure calculations using the GGA+U approach while only $Co_{1.50}Mn_{0.50}FeSi$ is predicted to be potential half-metal in GGA approach. The structural analysis reveals that the alloys crystallize in a cubic Heusler structure. A certain amount of disorder is observed in V and Ti substituted alloys. The magnetic properties were analyzed at both 5 and 300 K. The saturation magnetic moments of the alloys measured at 5 K are in fair agreement with those expected from Slater-Pauling rule. The results are also in accordance with the electronic structure calculations, indicating the half-metallicity and high spin polarization required for spintronics applications. The Curie temperatures of all compounds are higher than 700 K, allowing use at room temperature and above. Robust mechanical properties with hardness values increasing with the substitution of Y element and with its atomic radius are also observed. This manner of substitution of low-valence transition metal atoms to design new quaternary Heusler compounds gives enormous potential for many room temperature applications such as in spintronics or thermoelectrics and other areas of research, and clearly deserve further exploration on thin films in the future.

ACKNOWLEDGMENTS

We would like to acknowledge Dr. Mark Weaver for helpful discussions on measurements of mechanical properties and for providing the instrument for hardness measurements. This work utilizes the facilities offered by Central Analytical Facility (CAF) of University of Alabama. We are thus grateful to the members of CAF for helping us with measurements. The computational resources were provided by the UA High Performance Computing Facility (UAHPC). The financial support to conduct this work was sourced from NSF DMREF Grant No. 1235396, and NSF DMR Grant No. 1508680. The authors are thankful to NSF for providing the support to carry out this work.

[1] T. Hahn, The 230 space groups, in *International Tables for Crystallography Volume A: Space-Group Symmetry* (Springer, Berlin, 2006), pp. 112–717.

[2] M. J. Mehl, D. Hicks, C. Toher, O. Levy, R. M. Hanson, G. Hart, and S. Curtarolo, The AFLOW library of crystallographic prototypes: Part 1, Comput. Mater. Sci. **136**, S1 (2017).

[3] R. A. de Groot, F. M. Mueller, P. G. van Engen, and K. H. J. Buschow, New Class of Materials: Half-Metallic Ferromagnets, Phys. Rev. Lett. **50**, 2024 (1983).

[4] I. Galanakis, P. H. Dederichs, and N. Papanikolaou, Slater-Pauling behavior and origin of the half-metallicity of the full-Heusler alloys, Phys. Rev. B **66**, 174429 (2002).

[5] S. Wurmehl, G. H. Fecher, H. C. Kandpal, V. Ksenofontov, C. Felser, and H.-J. Lin, Investigation of Co_2FeSi: The Heusler compound with highest Curie temperature and magnetic moment, Appl. Phys. Lett. **88**, 032503 (2006).

[6] P. Brown, K.-U. Neumann, P. Webster, and K. Ziebeck, The magnetization distributions in some Heusler alloys proposed as half-metallic ferromagnets, J. Phys.: Condens. Matter **12**, 1827 (2000).

[7] A. Yamasaki, S. Imada, R. Arai, H. Utsunomiya, S. Suga, T. Muro, Y. Saitoh, T. Kanomata, and S. Ishida, Orbital angular momentum and interpretation of core-absorption magnetic circular dichroism on the band picture in Co-based Heusler alloys Co_2YSn(Y = Ti,Zr, and Nb), Phys. Rev. B **65**, 104410 (2002).

[8] T. Graf, C. Felser, and S. S. Parkin, Simple rules for the understanding of Heusler compounds, Prog. Solid State Chem. **39**, 1 (2011).

[9] C. Felser and A. Hirohata, *Heusler Alloys* (Springer, Berlin, 2015).

[10] S. Karthik, A. Rajanikanth, T. Nakatani, Z. Gercsi, Y. Takahashi, T. Furubayashi, K. Inomata, and K. Hono, Effect of Cr substitution for Fe on the spin polarization of $Co_2Cr_xFe_{1-x}Si$ Heusler alloys, J. Appl. Phys. **102**, 043903 (2007).

[11] N. Tezuka, N. Ikeda, S. Sugimoto, and K. Inomata, Giant tunnel magnetoresistance at room temperature for junctions using full-Heusler $Co_2FeAl_{0.5}Si_{0.5}$ electrodes, Jpn. J. Appl. Phys. **46**, L454 (2007).

[12] B. C. S. Varaprasad, A. Rajanikanth, Y. Takahashi, and K. Hono, Enhanced spin polarization of Co_2MnGe Heusler alloy by substitution of Ga for Ge, Appl. Phys. Express **3**, 023002 (2010).

[13] T. Nakatani, A. Rajanikanth, Z. Gercsi, Y. Takahashi, K. Inomata, and K. Hono, Structure, magnetic property, and spin polarization of $Co_2FeAl_xSi_{1-x}$ Heusler alloys, J. Appl. Phys. **102**, 033916 (2007).

[14] B. Deka, A. Srinivasan, R. Singh, B. C. S. Varaprasad, Y. Takahashi, and K. Hono, Effect of Co substitution for Mn on spin polarization and magnetic properties of ferrimagnetic Mn_2VAl, J. Alloys Compd. **662**, 510 (2016).

[15] B. C. S. Varaprasad, A. Srinivasan, Y. Takahashi, M. Hayashi, A. Rajanikanth, and K. Hono, Spin polarization and Gilbert damping of $Co_2Fe(Ga_xGe_{1-x})$ Heusler alloys, Acta Mater. **60**, 6257 (2012).

[16] K. Özdoğan, B. Aktaş, I. Galanakis, and E. Şaşıoğlu, Influence of mixing the low-valent transition metal atoms (Y, $Y^* = Cr$, Mn, Fe) on the properties of the quaternary Co_2 $[Y_{1-x}Y^*_x]$ Z (Z = Al, Ga, Si, Ge, or Sn) Heusler compounds, J. Appl. Phys. **101**, 073910 (2007).

[17] I. Galanakis, K. Özdoğan, B. Aktaş, and E. Şaşıoğlu, Effect of doping and disorder on the half metallicity of full Heusler alloys, Appl. Phys. Lett. **89**, 042502 (2006).

[18] R. Mahat, S. KC, U. Karki, J. Y. Law, V. Franco, I. Galanakis, A. Gupta, and P. LeClair, Possible half-metallic behavior of $Co_{2-x}Cr_xFeGe$ Heusler alloys: Theory and experiment, Phys. Rev. B **104**, 014430 (2021).

[19] S. KC, R. Mahat, S. Regmi, A. Mukherjee, P. Padhan, R. Datta, W. H. Butler, A. Gupta, and P. LeClair, Tunable properties and potential half-metallicity in $(Co_{2-x}Ti_x)FeGe$ Heusler alloys: An experimental and theoretical investigation, Phys. Rev. Materials **3**, 114406 (2019).

[20] R. Mahat, S. KC, U. Karki, S. Regmi, J. Y. Law, V. Franco, I. Galanakis, A. Gupta, and P. LeClair, Structural, electronic, magnetic, transport and mechanical properties of the half-metal-type quaternary Heusler alloy $Co_2Fe_{1-x}V_xGe$, J. Magn. Magn. Mater. **539**, 168352 (2021).

[21] H. C. Kandpal, G. H. Fecher, C. Felser, and G. Schönhense, Correlation in the transition-metal-based Heusler compounds Co_2MnSi and Co_2FeSi, Phys. Rev. B **73**, 094422 (2006).

[22] B. Balke, G. H. Fecher, H. C. Kandpal, C. Felser, K. Kobayashi, E. Ikenaga, J.-J. Kim, and S. Ueda, Properties of the quaternary half-metal-type Heusler alloy $Co_2Mn_{1-x}Fe_xSi$, Phys. Rev. B **74**, 104405 (2006).

[23] G. H. Fecher and C. Felser, Substituting the main group element in cobalt-iron based Heusler alloys: $Co_2FeAl_{1-x}Si_x$, J. Phys. D **40**, 1582 (2007).

[24] Y. Du, G. Xu, X. Zhang, Z. Liu, S. Yu, E. Liu, W. Wang, and G. Wu, Crossover of magnetoresistance in the zero-gap half-metallic Heusler alloy Fe_2CoSi, Europhys. Lett. **103**, 37011 (2013).

[25] C. Sterwerf, S. Paul, B. Khodadadi, M. Meinert, J.-M. Schmalhorst, M. Buchmeier, C. K. Mewes, T. Mewes, and G. Reiss, Low Gilbert damping in Co_2FeSi and Fe_2CoSi films, J. Appl. Phys. **120**, 083904 (2016).

[26] L. Bainsla, A. I. Mallick, M. M. Raja, A. K. Nigam, B. S. D. C. S. Varaprasad, Y. K. Takahashi, A. Alam, K. G. Suresh, and K. Hono, Spin gapless semiconducting behavior in equiatomic quaternary CoFeMnSi Heusler alloy, Phys. Rev. B **91**, 104408 (2015).

[27] L. Bainsla, K. Z. Suzuki, M. Tsujikawa, H. Tsuchiura, M. Shirai, and S. Mizukami, Magnetic tunnel junctions with an equiatomic quaternary CoFeMnSi Heusler alloy electrode, Appl. Phys. Lett. **112**, 052403 (2018).

[28] X. Dai, G. Liu, G. H. Fecher, C. Felser, Y. Li, and H. Liu, New quarternary half metallic material CoFeMnSi, J. Appl. Phys. **105**, 07E901 (2009).

[29] Y. Jin, P. Kharel, P. Lukashev, S. Valloppilly, B. Staten, J. Herran, I. Tutic, M. Mitrakumar, B. Bhusal, A. O'Connell *et al.*, Magnetism and electronic structure of CoFeCrX (X= Si, Ge) Heusler alloys, J. Appl. Phys. **120**, 053903 (2016).

[30] L. Xiong, L. Yi, and G. Gao, Search for half-metallic magnets with large half-metallic gaps in the quaternary Heusler alloys CoFeTiZ and CoFeVZ (Z= Al, Ga, Si, Ge, As, Sb), J. Magn. Magn. Mater. **360**, 98 (2014).

[31] Y. Zhang, Z. Liu, G. Li, X. Ma, and G. Liu, Magnetism, band gap and stability of half-metallic property for the quaternary Heusler alloys CoFeTiZ (Z= Si, Ge, Sn), J. Alloys Compd. **616**, 449 (2014).

[32] I. Galanakis, P. H. Dederichs, and N. Papanikolaou, Origin and properties of the gap in the half-ferromagnetic Heusler alloys, Phys. Rev. B **66**, 134428 (2002).

[33] https://periodictable.com/Properties/A/AtomicRadius.v.html.

[34] M. Wójcik, E. Jedryka, H. Sukegawa, T. Nakatani, and K. Inomata, ^{59}Co NMR experiment as a probe of electron doping in $Co_2FeAl_{1-x}Si_x$ Heusler alloys, Phys. Rev. B **85**, 100401(R) (2012).

[35] T. Kubota, S. Tsunegi, M. Oogane, S. Mizukami, T. Miyazaki, H. Naganuma, and Y. Ando, Half-metallicity and Gilbert damping constant in $Co_2Fe_xMn_{1-x}Si$ Heusler alloys depending on the film composition, Appl. Phys. Lett. **94**, 122504 (2009).

[36] R. Shan, H. Sukegawa, W. H. Wang, M. Kodzuka, T. Furubayashi, T. Ohkubo, S. Mitani, K. Inomata, and K. Hono, Demonstration of Half-Metallicity in Fermi-Level-Tuned Heusler Alloy $Co_2FeAl_{0.5}Si_{0.5}$ at Room Temperature, Phys. Rev. Lett. **102**, 246601 (2009).

[37] N. Tezuka, N. Ikeda, F. Mitsuhashi, and S. Sugimoto, Improved tunnel magnetoresistance of magnetic tunnel junctions with Heusler $Co_2FeAl_{0.5}Si_{0.5}$ electrodes fabricated by molecular beam epitaxy, Appl. Phys. Lett. **94**, 162504 (2009).

[38] G. H. Fecher, H. C. Kandpal, S. Wurmehl, C. Felser, and G. Schönhense, Slater-Pauling rule and Curie temperature of Co_2-based Heusler compounds, J. Appl. Phys. **99**, 08J106 (2006).

[39] K. Kobayashi, R. Umetsu, R. Kainuma, K. Ishida, T. Oyamada, A. Fujita, and K. Fukamichi, Phase separation and magnetic properties of half-metal-type $Co_2Cr_{1-x}Fe_xAl$ alloys, Appl. Phys. Lett. **85**, 4684 (2004).

[40] R. Y. Umetsu, K. Kobayashi, A. Fujita, K. Oikawa, R. Kainuma, K. Ishida, N. Endo, K. Fukamichi, and A. Sakuma, Half-metallic properties of $Co_2(Cr_{1-x}Fe_x)Ga$ Heusler alloys, Phys. Rev. B **72**, 214412 (2005).

[41] Y. Miura, K. Nagao, and M. Shirai, Atomic disorder effects on half-metallicity of the full-Heusler alloys $Co_2(Cr_{1-x}Fe_x)Al$: A first-principles study, Phys. Rev. B **69**, 144413 (2004).

[42] I. Galanakis, Appearance of half-metallicity in the quaternary Heusler alloys, J. Phys.: Condens. Matter **16**, 3089 (2004).

[43] R. Mahat, K. Shambhu, D. Wines, F. Ersan, S. Regmi, U. Karki, R. White, C. Ataca, P. Padhan, A. Gupta, and P. LeClair, Tuneable structure and magnetic properties in $Fe_{3-x}V_xGe$ alloys, J. Alloys Compd. **830**, 154403 (2020).

[44] R. Mahat, S. KC, D. Wines, S. Regmi, U. Karki, Z. Li, F. Ersan, J. Law, C. Ataca, V. Franco, A. Gupta, and P. LeClair, Influence of Cr-substitution on the structural, magnetic, electron transport, and mechanical properties of $Fe_{3x}Cr_xGe$ Heusler alloys, J. Magn. Magn. Mater. **521**, 167398 (2021).

[45] C. Boudias and D. Monceau, *CaRIne Crystallography: The Crystallographic Software for Research and Teaching* (CaRIne Crystallography, 2006).

[46] P. LeClair, X-ray Diffraction Calculation Software (2018).

[47] Match! - Phase Analysis using Powder Diffraction, Version 3.x, Crystal Impact - Dr. H. Putz and Dr. K. Brandenburg GbR, Kreuzherrenstr. 102, 53227 Bonn, Germany, https://www.crystalimpact.de/match.

[48] P. E. Blöchl, Projector augmented-wave method, Phys. Rev. B **50**, 17953 (1994).

[49] G. Kresse and J. Furthmüller, Efficient iterative schemes for *ab initio* total-energy calculations using a plane-wave basis set, Phys. Rev. B **54**, 11169 (1996).

[50] J. P. Perdew, K. Burke, and M. Ernzerhof, Generalized Gradient Approximation Made Simple, Phys. Rev. Lett. **77**, 3865 (1996).

[51] H. J. Monkhorst and J. D. Pack, Special points for Brillouin-zone integrations, Phys. Rev. B **13**, 5188 (1976).

[52] P. Mavropoulos, I. Galanakis, V. Popescu, and P. Dederichs, The influence of spin–orbit coupling on the band gap of Heusler alloys, J. Phys.: Condens. Matter **16**, S5759 (2004).

[53] E. Şaşıoğlu, I. Galanakis, C. Friedrich, and S. Blügel, Calculated electronic and magnetic properties of the half-metallic, transition metal based Heusler compounds, Phys. Rev. B **88**, 134402 (2013).

[54] H. C. Kandpal, G. H. Fecher, and C. Felser, Calculated electronic and magnetic properties of the half-metallic, transition metal based Heusler compounds, J. Phys. D **40**, 1507 (2007).

[55] H. S. Nalwa, *Handbook of Nanostructured Materials and Nanotechnology, Five-Volume Set* (Academic, New York, 1999).

[56] M. Che and J. C. Védrine, (John Wiley and Sons, New York, 2012).

[57] See Supplemental Material at http://link.aps.org/supplemental/10.1103/PhysRevMaterials.6.064413 for more detailed information regarding crystal structure, magnetic measurements, and band calculations.

[58] P. Webster, Magnetic and chemical order in Heusler alloys containing cobalt and manganese, J. Phys. Chem. Solids **32**, 1221 (1971).

[59] T. J. Burch, T. Litrenta, and J. I. Budnick, Hyperfine Studies of Site Occupation in Ternary Systems, Phys. Rev. Lett. **33**, 421 (1974).

[60] Enamullah, Y. Venkateswara, S. Gupta, M. R. Varma, P. Singh, K. G. Suresh, and A. Alam, Electronic structure, magnetism, and antisite disorder in CoFeCrGe and CoMnCrAl quaternary Heusler alloys, Phys. Rev. B **92**, 224413 (2015).

[61] P. Webster and K. Ziebeck, Magnetic and chemical order in Heusler alloys containing cobalt and titanium, J. Phys. Chem. Solids **34**, 1647 (1973).

[62] W. Hume-Rothery, Researches on the Nature, Properties, and Conditions of Formation of Intermetallic Compounds, with Special Reference to Certain Compounds of tin, Ph.D. thesis, University of London, 1926.

[63] A.-P. Tsai, A test of Hume-Rothery rules for stable quasicrystals, J. Non-Cryst. Solids **334-335**, 317 (2004).

[64] M.-x. Ren, B.-s. Li, and H.-z. Fu, Formation condition of solid solution type high-entropy alloy, Trans. Nonferrous Metals Soc. China **23**, 991 (2013).

[65] J. E. Fischer, J. Karel, S. Fabbrici, P. Adler, S. Ouardi, G. H. Fecher, F. Albertini, and C. Felser, Magnetic properties and Curie temperatures of disordered Heusler compounds: $Co_{1+x}Fe_{2-x}Si$, Phys. Rev. B **94**, 024418 (2016).

[66] B. Cullity and S. Stock, *Elements of X-Ray Diffraction: Pearson New International*, 3rd ed. (Pearson, Essex, 2014).

[67] A. R. Denton and N. W. Ashcroft, Vegard's law, Phys. Rev. A **43**, 3161 (1991).

[68] T. Block, M. J. Carey, B. A. Gurney, and O. Jepsen, Band-structure calculations of the half-metallic ferromagnetism and structural stability of full- and half-Heusler phases, Phys. Rev. B **70**, 205114 (2004).

[69] A. Arrott, Criterion for ferromagnetism from observations of magnetic isotherms, Phys. Rev. **108**, 1394 (1957).

[70] K. Srinivas, T. Prasanna Kumari, M. Manivel Raja, and S. Kamat, Effect of Fe substitution for Co on structure, electrical resistivity, and magnetic properties of Heusler type $Co_{2-x}Fe_{1+x}Si$ alloys, J. Appl. Phys. **114**, 033911 (2013).

[71] M. Hakimi, P. Kameli, H. Salamati, and Y. Mazaheri, Evolution of microstructural and mechanical properties of nanocrystalline Co_2FeAl Heusler alloy prepared by mechanical alloying, Powder Metall. **56**, 111 (2013).

[72] S. Ouardi, G. H. Fecher, B. Balke, A. Beleanu, X. Kozina, G. Stryganyuk, C. Felser, W. Klöß, H. Schrader, F. Bernardi, J. Morais, E. Ikenaga, Y. Yamashita, S. Ueda, and K. Kobayashi, Electronic and crystallographic structure, hard x-ray photoemission, and mechanical and transport properties of the half-metallic Heusler compound Co_2MnGe, Phys. Rev. B **84**, 155122 (2011).

[73] R. Mahat, S. K.C., U. Karki, S. Regmi, J. Y. Law, V. Franco, I. Galanakis, A. Gupta, and P. Leclair, Structural, electronic, magnetic, and mechanical properties of $Co_{2-x}V_xFeSi$ Heusler alloys, IEEE Trans. Magn. **58**, 1 (2022).

[74] G. Rogl, A. Grytsiv, M. Gürth, A. Tavassoli, C. Ebner, A. Wünschek, S. Puchegger, V. Soprunyuk, W. Schranz, E. Bauer *et al.*, Mechanical properties of half-Heusler alloys, Acta Mater. **107**, 178 (2016).

[75] A. van de Walle, P. Tiwary, M. De Jong, D. Olmsted, M. Asta, A. Dick, D. Shin, Y. Wang, L.-Q. Chen, and Z.-K. Liu, Efficient stochastic generation of special quasirandom structures, Calphad **42**, 13 (2013).

[76] A. van de Walle, M. Asta, and G. Ceder, The alloy theoretic automated toolkit: A user guide, Calphad **26**, 539 (2002).

[77] A. van de Walle, Alloy Theoretic Automated Toolkit (ATAT): A User Guide, (2019), https://www.brown.edu/Departments/Engineering/Labs/avdw/atat/manual.pdf.

[78] K. Özdoğan, I. V. Maznichenko, S. Ostanin, E. Şaşıoğlu, A. Ernst, I. Mertig, and I. Galanakis, High spin polarization in

all-3d-metallic Heusler compounds: the case of Fe_2CrZ and Co_2CrZ (Z = Sc, Ti, V), J. Phys. D **52**, 205003 (2019).

[79] I. Galanakis, Towards half-metallic interfaces: Co_2CrAl/InP contacts, J. Phys.: Condens. Matter **16**, 8007 (2004).